MDPI

Article

Study on the Stability of Coal Pillars in a Gob-Side Two-Entry Arrangement of Different Layers in Fully Mechanized Caving and the Zonal Linkage Control of "Heteromorphic" Surrounding Rock

Hui Li [1], Sheng Gao [2], Dongdong Chen [1], Shengrong Xie [1,*], Yiyi Wu [1], Shaohua Feng [1], Zaisheng Jiang [1] and Fangfang Guo [1]

1 School of Energy and Mining Engineering, China University of Mining and Technology-Beijing, Beijing 100083, China; lihuiywwq@163.com (H.L.); chendongbcg@163.com (D.C.); 15662045768@163.com (Y.W.); fshahsx@163.com (S.F.); jzs13391782857@163.com (Z.J.); gffever@163.com (F.G.)
2 CCTEG Energy Technology Development Co., Ltd., Beijing 100013, China; 18810979386@163.com
* Correspondence: xsrxcq@cumtb.edu.cn; Tel.: +86-13810521426

Abstract: To solve the problem of considerable deformation of the tailgate in a fully mechanized caving face, the position of the main roof fracture line is first obtained by theoretical calculation, combined with the results of a similar simulation test and numerical simulation analysis. The width of the section coal pillar in the tailgate is determined to be 11.5 m. Based on the distribution characteristics of deviatoric stress and the plastic zone of surrounding rock, combined with the location characteristics and geological conditions, a new zoning control design approach is proposed, a "two pillars, three zones, and three parts" arrangement for the surrounding rock of the tailgate. The targeted two-entry support design is carried out following common engineering practices. Mine pressure monitoring data were used to verify the results of the new two-entry design. The comparison shows that the supporting technology can effectively control the considerable deformation of the surrounding rock, improving stability for regular mining production.

Keywords: gob-side entry driving (GED); broken coal; section coal pillar width; grouting; roadway surrounding rock control

1. Introduction

With the decrease in fossil energy use and the continuous increase in the proportion of renewable energy in the national energy structure [1–5], high production and efficiency have gradually become the core index of green coal mining in China. This investigation shows that coal loss caused by wide coal pillar roadway protection ranks first among the reasons for wastage of coal resources in China [6]. To reduce the loss of section coal pillars and improve the coal recovery rate, gob-side entry driving (GED) technology has been widely used in mining [7]. However, the GED coal pillar causes further problems with the increasing intensity and depth of coal mining and the gradual deterioration of the mining environment [7–9], such as considerable deformation and instability. The stability of the section coal pillar is critical to the safe implementation of GED.

Scholars have extensively researched the surrounding rock stability and control technology of GED. Hou et al. [10] proposed the stability principle of the large and small structures of surrounding rocks for GED in fully mechanized caving. They considered that the key block of the main roof arc triangle plays a decisive role in the stability of gob-side entry. According to the characteristics of mine pressure distribution in fully mechanized caving faces and the bolt support that enhances the strength of the surrounding rocks, Bai et al. [11] expounded the surrounding rock control mechanism of GED. He et al. [12] studied the severe deformation of the surrounding rocks during GED mining with a thick

and hard main roof, and used field measurement and theoretical calculation to determine the fracture position of the main roof and reasonable coal pillar width; they also studied the roadway deformation mechanism and proposed a joint control technology for GED with a thick and hard main roof. Hua et al. [13,14] discovered a surrounding rock control mechanism for GED with a narrow coal pillar in an isolated working face by studying the mine pressure behavior characteristics and the elastic strain energy density dissipation law for different coal pillar widths in the isolated working face, and proposed the countermeasures for targeted surrounding rock control. Wang et al. [15–17] analyzed the deformation and failure characteristics of surrounding roadway rock, revealed the deformation and failure mechanisms of the surrounding rock, and provided the corresponding support scheme according to different geological conditions. Zhang et al. [18,19] used a mine borehole observation instrument to observe the roof rock and the narrow coal pillar of the GED under an overburden, proposed a statistical method of borehole fractures, studied and analyzed the fracture distribution law, and determined the control technology. Zhang et al. [20] presented a two-step GED technology of replacing the narrow coal pillars with a pre-built artificial roadway side composed of gangue. In addition, there has been significant research on surrounding rock stability and control technology for GEDs under various complex conditions, such as extra-thick coal seams [21–23], heading for adjacent advancing coal faces [24], and deeply inclined coal seams [25–27].

The width of the coal pillar is an essential factor affecting the stability of the surrounding rock of the GED in fully mechanized caving. According to Bai et al. [28], a stress-relaxed area is formed in the solid side coal after mining, which provides favorable conditions for the layout of GED. Li et al. [29] established the structural mechanics model of GED by using the theoretical analysis method, deducing the expression of the width of the "internal stress field" and determining the proper position of the GED. Yu et al. [30] inferred a reasonable presentation of narrow coal pillar width, while Xie et al. [31] pointed out that the suitable width of roadway pillars should be less than the critical width of stress transfer from the solid coal in the roadway side to the coal pillar. Research on reasonable coal pillar width has always focused on surrounding rock control and efficient mining of coal resources [32,33].

High-drainage roadways and tailgates are usually arranged in the rock stratum or coal seam on one side of the panel, and the distance between the two roadways is close, forming a system of two entries in different layers to prevent gas accumulation in the upper corner of the panel in high-gas mines. When the GED in fully mechanized caving adopts a two-entry system in different layers, the adjacent gob coal roadway at the lower position experiences the interaction of the lateral abutment pressure of the adjacent gob, the advancing abutment pressure of the isolated panel, and the superposition stress of the two roadways, further aggravating the deformation, failure, and instability of the surrounding rock [34]. Based on theoretical calculations, laboratory tests, and numerical simulations, combined with field-measured results, this study explores and analyzes the reasonable coal pillar width for GED in fully mechanized caving and explains the failure mechanism of the surrounding rock of the adjacent gob roadway under two-entry conditions in different layers. This study then proposes the idea ("two pillars, three zones, and three parts") of graded and zoned support of surrounding rock of the two-entry sections in different layers, forming a specific support scheme. It has also been successfully field-tested in the tailgate of panel 3210 in the Wangpo mine, achieving the purpose of safe and efficient mining. At the same time, to solve other similar engineering problems, the zoning control design approach to solve these problems is provided, which provides theoretical support for practical engineering research.

2. Engineering Background

2.1. Project Overview

Wangpo mine is a high-gas mine located in Zezhou County, Jincheng City, Shanxi Province, China. At present, it mainly mines coal seam No. 3, with an average buried depth of 560 m, a coal seam thickness of 4.1–6.7 m, an average thickness of 5.76 m, a coal seam

dip angle of 2–12°, and an average dip angle of 6°. Mainly anthracite is found in the mine, with the coal body presenting fragmentation characteristics, and the cracks of the coal body are thoughtfully developed. Panel3210 is a fully mechanized isolated caving panel with a mining height of 3.0 m and a caving height of 2.76 m. The roof is managed by natural caving. The strike length of the panel is 2150 m, and the dip length is 159 m. The panels on both sides are mined. In 2018, the mine measured a relative gas emission quantity of 15.15 m^3/t, and the absolute gas was 104.84 m^3/min. A"U + I" type ventilation mode has been adopted for panel 3210. The tailgate and high-drainage roadway were arranged close to gob 3212.

The tailgate and high-drainage roadway were arranged in an internal staggered layout. The high-drainage roadway is placed in the roof rock layer, the tailgate is set along the coal seam roof, which is about 2.0 m away from the floor of the high-drainage roadway, and the coal pillar width between the high-drainage roadway and the tailgate is 6.0 m, forming a two-entry layout adjacent to the gob and different layers in the fully mechanized caving area (as shown in Figure 1a). The mining arrangement near the panel and the columnar structure of the coal and rock strata are shown in Figure 1.
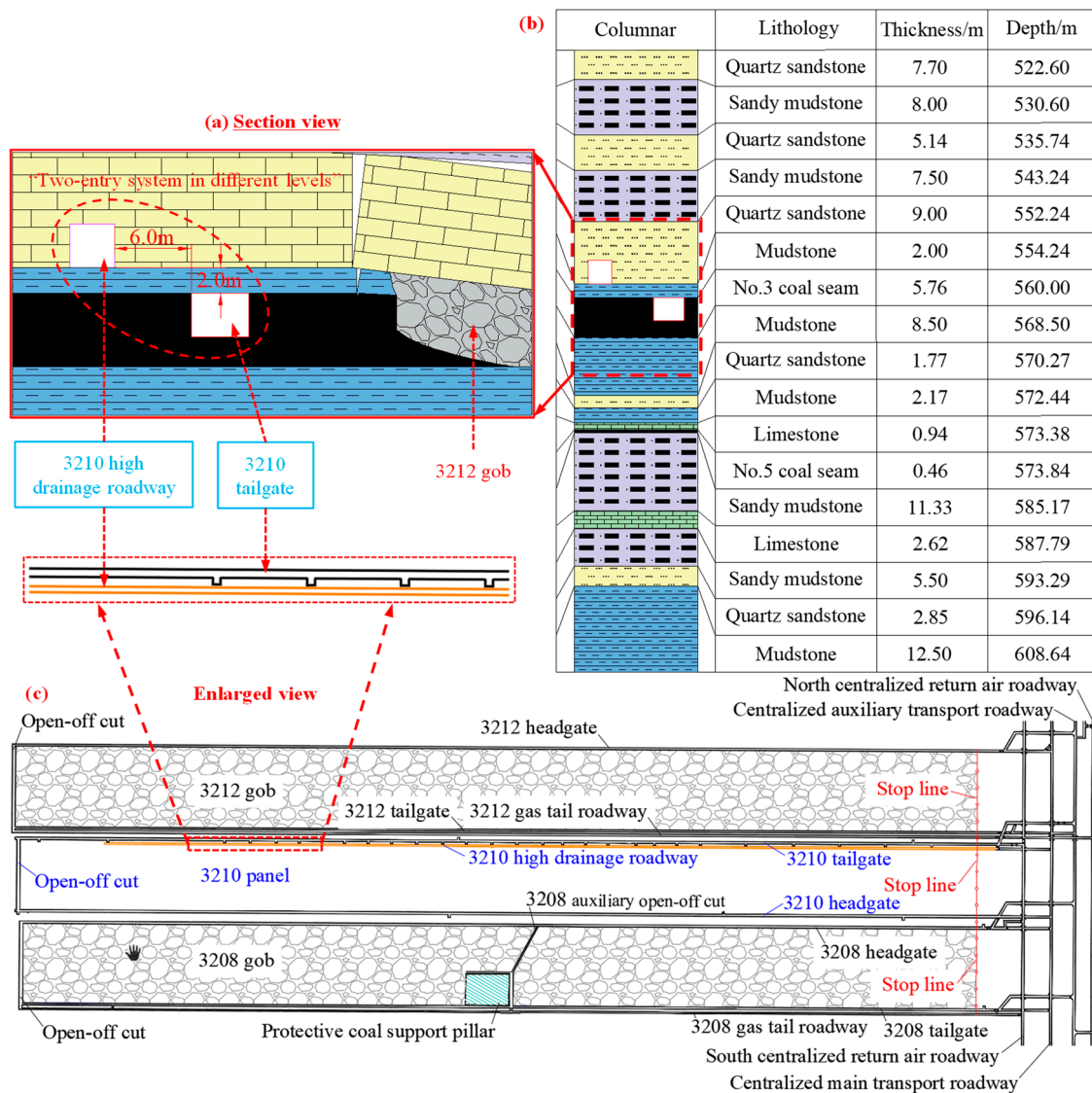

Figure 1. Location of panel 3210 and columnar characteristics of the coal and rock strata: (**a**) layout of the double entry in different layers, (**b**) column of the coal-rock strata, (**c**) location of panel 3210.

2.2. Observation of Surrounding Rock Structure and Analysis of Roadway Deformation Factors

Tailgate 3210 of the Wangpo mine belongs to the adjacent gob coal roadway excavated in the broken coal body. The support body was seriously damaged during the roadway service, and the maximum deformation of the rock surrounding the roadway is up to 1.5 m, as shown in Figure 2.
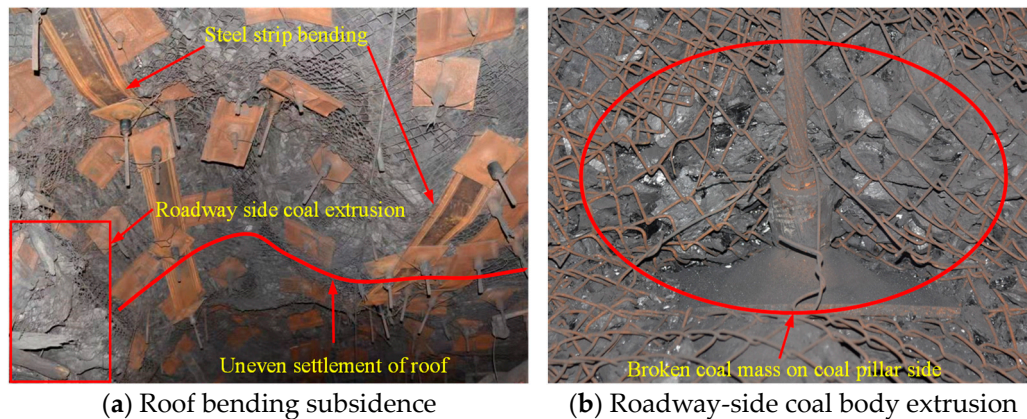
Figure 2. Deformation and failure of surrounding rock and support in tailgate 3210.

Previous research has shown that there are many discontinuous structural planes in coal and rock masses that have a significant impact on their deformation, failure, and mechanical properties, and the control effect of the rock mass structure on the mechanical properties of the rock mass are far more significant than those of rock materials [35]. A detailed understanding of the internal structure of the coal-and-rock mass plays a vital role in studying its deformation and mechanical properties. After the excavation and support of the tailgate, a small-aperture panoramic mine borehole observation instrument was selected to observe the surrounding rock structure. The test location was located at 650 m of tailgate 3210. The observation equipment and the results are presented in Figure 3.

As shown in Figure 3, the integrity of the roof rock strata is acceptable. There are visible cracks in the glimpsed section, mainly because the main roof of the tailgate is composed of a 9.0 m thick hard quartz sandstone, which can be seen from the two sides of the tailgate. The coal body in the depth range of 0–9.4 m on the solid coal side is slightly broken and has poor integrity, especially in the depth range of 0–4.0 m, which is the most broken and needs critical support. Within the depth range of 0–7.0 m at the side of the coal pillar, the coal fissure is developed and visible (the hole collapse at deeper depth cannot be glimpsed), and its integrity is poor. The coal pillar needs modified support to enhance its integrity.

According to the field investigation and observation results of the surrounding rock structure, the main factors inducing the surrounding rock instability of tailgate 3210 are as follows: 1. The fragmentation characteristics of the coal body, due to which the internal fissures of the coal bodies have been thoughtfully developed. At the same time, the coal seam accepts bedding and drilling for pre-gas drainage, and many drilling holes are intensively constructed that aggravate the degree of coal fragmentation further and reduce the strength of the coal body; 2. The mining of adjacent panels causes the plastic failure of the coal near tailgate 3210, and the lateral abutment pressure in the gob continuously impacts the coal in this area; 3. The strong disturbance of the advancing abutment pressure on the rock surrounding the roadway in the fully mechanized caving isolated panel quickly causes the instability of block B and the key block of the main roof in the adjacent gob. It affects the stability of the coal pillar or roadway under the key block. Therefore, a reasonable coal pillar section width is one of the critical factors for the stability of tailgate 3210; 4. The layout of the two entries along the gob is conducive to the discharge of gas from the gob and the upper corner. Still, due to its compact spatial arrangement, superposition stress

affects the two entries. As shown in Figure 4, the broken section coal pillar N and coal–rock pillar M between the two entries form weak coal–rock pillars with asymmetrical strength on both sides of tailgate 3210, which significantly impacts the stability of the tailgate.
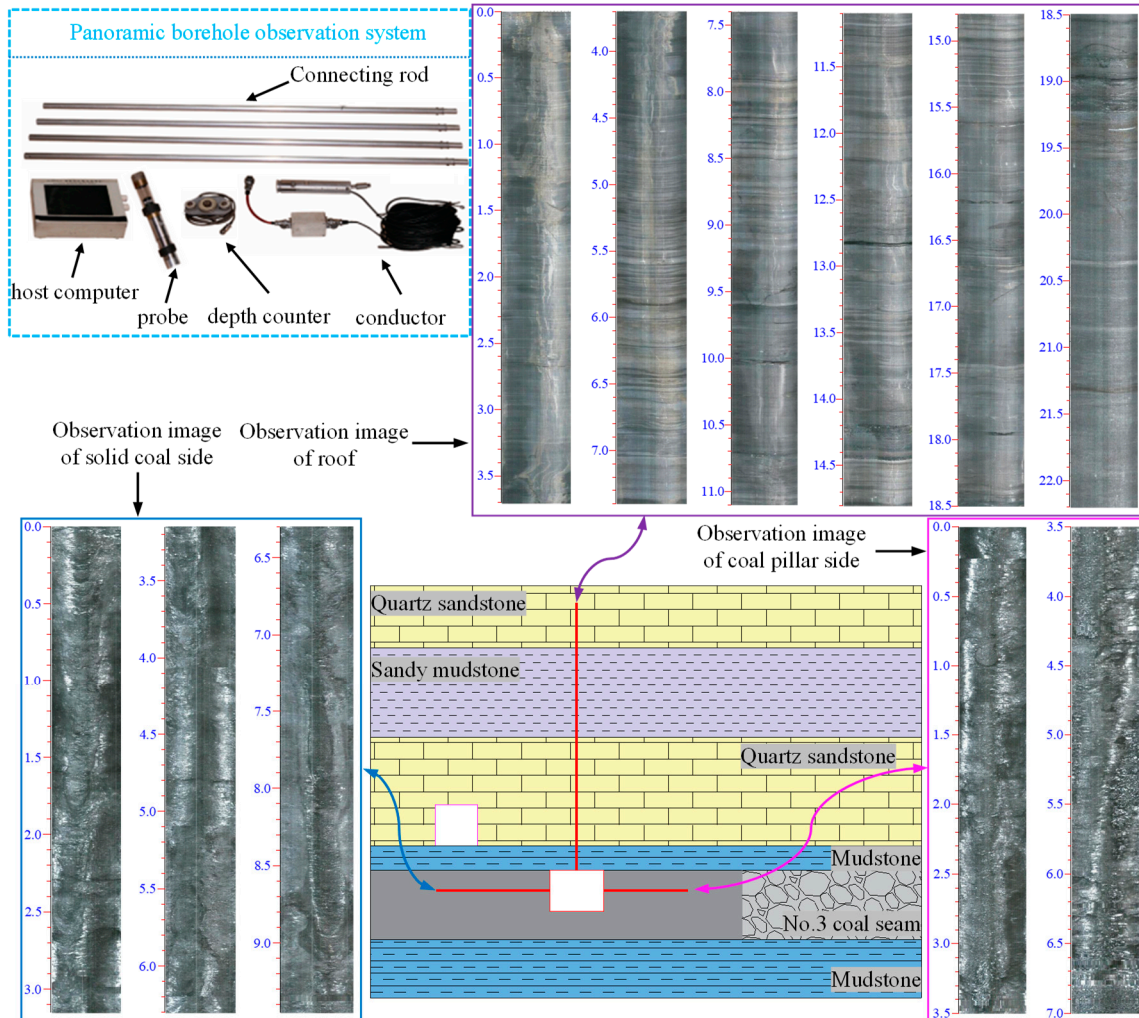

Figure 3. The observation equipment and results of the surrounding rock structure of tailgate 3210.
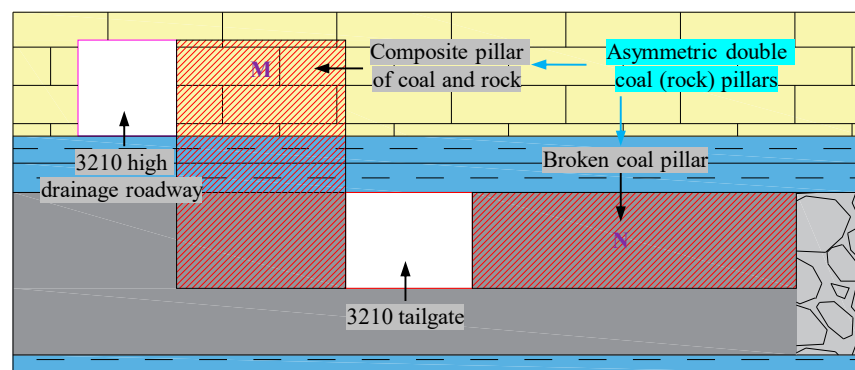

Figure 4. Weak, asymmetrically strong coal–rock pillars formed by the two-entry arrangement along with the gob.

In addition, the Wangpo mine is a high-gas mine, and the coal seam is mined by fully mechanized caving, resulting in more coal remaining in the gob. Coal seam fissures were developed and the air permeability was adequate. To reduce the influence of residual

coal gas in the adjacent gob on this panel, the air leakage of the coal pillar should be fully considered.

3. Determination of Coal Pillar Width in a Fully Mechanized Caving Face

3.1. Calculation of Reasonable Coal Pillar Width Based on Fracture Position of the Main Roof

As shown in Figure 5, after mining adjacent panels, the key rock strata (main roof) located in the roof of the coal seam break above the coal body on the side of the gob to form arc triangle B [11,36]. The arc triangle significantly impacts the stability of the surrounding rock of the gob-side entry. After the rotation of block B, one end touches the gangue in the gob, and the other end breaks on the solid coal. Due to the strong support of solid coal, the immediate roof, and caving gangue, block B is relatively stable. Geological data shows a 5.14 m thick hard quartz sandstone layer at 7.5 m above the main roof. Because the coal seam is thick, coal seam mining has an extensive disturbance range to the overlying strata. This layer of quartz sandstone also breaks above the solid coal at the side of the gob to form a stable arc triangle B′ because it is close to the coal seam. Block B's instability will also affect the stability of the coal or the surrounding roadway rock below. The two arc triangle blocks (called middle- and low-position arc triangle blocks) above the solid coal on the side of the gob may be broken or even broken simultaneously owing to the disturbance of the gob-side entry and the advancing abutment pressure of the mining face. If the two arc triangle blocks break simultaneously, they will cause severe damage to the coal or surrounding roadway rock below and are very prone to accidents. Therefore, the tailgate should be arranged within the fracture line of the lower arc triangle block B.
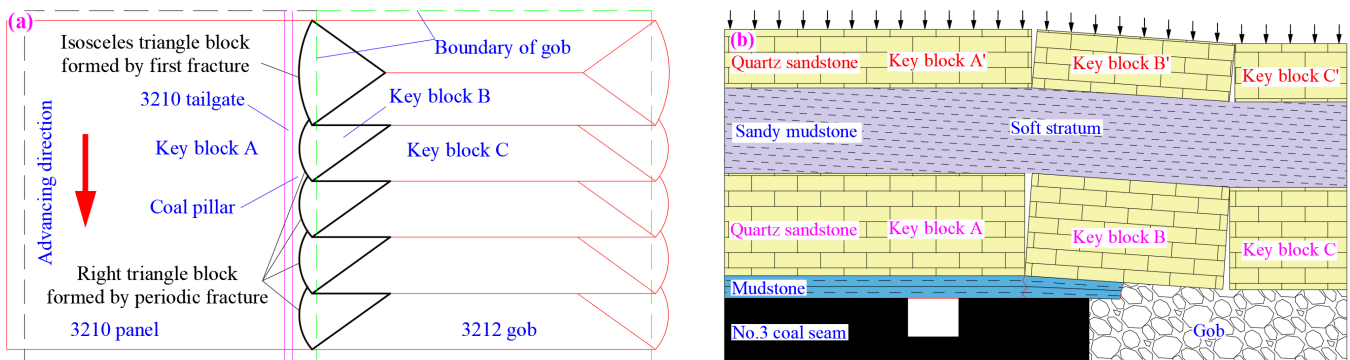
Figure 5. Roof rock strata arc triangle structures of tailgate 3210. (**a**) Key arc triangle structure; (**b**) middle- and low-position arc triangle structures of the tailgate.

1.　Determining the fracture position of the main roof based on the theory of "internal and external stress fields"

According to the theory of "internal and external stress fields", the abutment pressure area is divided into two parts, with the fracture line as the boundary [37]; that is, the "internal stress field" is determined by the dead weight of the fractured rock beam between the fracture line and the coal wall and the "external stress field" is determined by the weight of the overlying strata outside the fracture line. The width S_1 is the calculated fracture line penetrating the coal body of the "internal stress field", and the abutment pressure F [37] distributed in the "internal stress field" is

$$F = \int_0^{s_1} \sigma_y \mathrm{d}x = \frac{G_0 y_0 S_1}{6} \tag{1}$$

where σ_y is the lateral abutment pressure, Pa, G_0 is the stiffness of plastic coal near the main roof fracture line, Pa, and y_0 is the average compression amount of coal at the coal wall, m.

The main roof weight before the first weighting of the panel is equal to the vertical stress distributed along the "internal stress field" of the coal around the gob, which can be obtained as follows:

$$F = \gamma abh \tag{2}$$

where γ is the average unit weight of the main roof, N/m^3, a is the length of the panel, m, b is the first weighting interval, m, and h is the height of the main roof.

The first weighting interval of the main roof can be obtained from the following formula [38]:

$$b = h\sqrt{\frac{2\sigma_t}{q}} \tag{3}$$

where σ_t is the tensile strength of the main roof, Pa, and q is the load on the main roof, Pa.

The load borne by the main roof includes its load and overburden weight. Considering the effect of the n-layer strata on the main roof, the burden borne by the main roof is [38]

$$(q_n)_1 = \frac{E_1 h_1^3 (\gamma_1 h_1 + \gamma_2 h_2 + \cdots + \gamma_n h_n)}{E_1 h_1^3 + E_2 h_2^3 + \cdots + E_n h_n^3} \tag{4}$$

The characteristics of each stratum of coal seam roof are as follows:

Substituting the data in Table 1 into Formula (4), it is calculated that $(q_4)_1$ = 320.2 kPa, $(q_5)_1$ = 317.4 kPa < $(q_4)_1$. The fourth layer of quartz sandstone above the main roof does not affect the main roof load because of its high strength and thick rock strata. Therefore, the load on the main roof is 320.2 kPa.

Table 1. Characteristics of each stratum of coal seam roof.

Sequence (n)	Rock Strata	Thickness/m	Bulk Density/(MN·m^{-3})	Elastic Modulus/GPa
5	Quartz sandstone	7.70	0.025	17.80
4	Sandy mudstone	8.00	0.024	15.00
3	Quartz sandstone	5.14	0.025	17.80
2	Sandy mudstone	7.50	0.024	15.00
Main roof (1)	Quartz sandstone	9.00	0.025	17.80
-	Mudstone	2.00	0.023	15.00
-	No. 3 coal seam	5.76	0.0144	12.08

Simultaneous Formulas (1)–(4) can be obtained:

$$S_1 = \frac{6\gamma a h^2}{G_0 y_0} \sqrt{\frac{2\sigma_t}{(q_4)_1}} \tag{5}$$

where γ = 25 × 10^3 N·m^{-3}, a = 159 m, h = 9 m, and σ_t = 2.1 MPa. The stiffness (G_0) of the plastic coal near the main roof fracture line is 1.2 GPa, and the average compression amount (y_0) is 0.8 m.

Substituting the above data into Formula (5), it is found that the width S_1 of the "internal stress field" is 7.29 m, and the width of the main roof fracture line penetrating the coal body is 7.29 m.

2. Verification of fracture position of main roof based on similarity simulation test

A laboratory test was carried out using the similarity simulation method to verify the fracture position of the main roof of the adjacent gob in the coal body and understand the overburden collapse form [39]. In this experiment, a two-dimensional simulation experimental table was used; the size of the table was length × thickness × height = 1800 mm × 160 mm × 1600 mm. This experiment simulated the actual coal and rock height of 150 m, the geometric similarity ratio was α_L = 150, and the unit weight similarity ratio

was $\alpha_\gamma = 1.5$. The height of the model was 1000 mm, in which the overburden thickness of the No. 3 coal seam was 119 m, the actual buried depth of the coal seam was 560 m, and the external pressure was 11.03 MPa to simulate the overburden load of 441 m. Combined with the size of the experimental table, the actual loading pressure in the model was 0.049 MPa.

As shown in Figure 6, after mining the 3212 panel, the 2 m thick mudstone on the immediate roof will fall with the mining, leading to the collapse of the overburden. The maximum separation height of the roof was up to 39.0 m. It can be directly observed that the key triangle block forms an articulated structure with the rock mass on the coal body and the rock mass on the gob; the lateral fracture span $L_1 = 13.89$ m and the included angle between the fracture line of the main roof and the horizontal direction was 58°. The fracture line was located about 6.77 m inside the coal wall, and the similarity simulation results are similar to the theoretical calculation values.
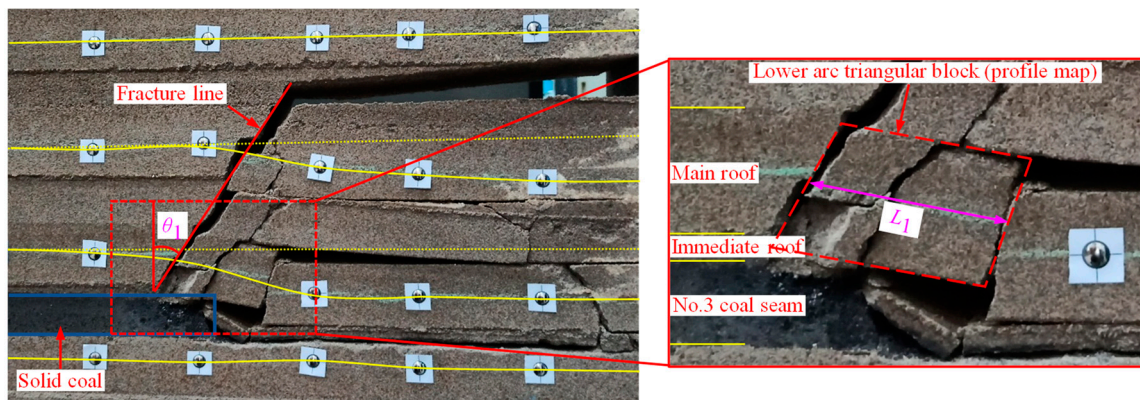
Figure 6. Collapsed form of end overburden and key block parameters of main roof. Yellow arrow/purple circle.

Combined with the above analysis, to avoid the damaging impact of the fracture and the instability of the arc triangle block on the lower coal body or the surrounding roadway rock, the tailgate should be arranged within the fracture line of the lower arc triangle block. In addition, considering the instability risk of the lower arc triangle block, the influence of mining roadway excavation on the coal pillar, effective support distance of the anchor bolt in the tailgate, uneven coal strength, gob gas, ponding, and rib spalling on the coal pillar stability should also be considered. To effectively ensure the stability of the coal pillar, a sufficient safety distance should be reserved between the fracture line of the lower arc triangle block and the side of the tailgate, which mainly includes two parts: ensuring the effective support range of the coal body (effective length of anchor bolt x_1), and considering the safety factor of the project (surplus length x_2). Therefore, the width of the coal pillar should satisfy the following:

$$L \geq x_1 + x_2 + S_1 \tag{6}$$

The effective length x_1 of the anchor bolt is 2.4 m and the safety margin length of the coal pillar width x_2 is $0.10(x_1 + S_1) = 0.97$ m. The value of S_1 is 7.29 m, and L is calculated to be ≥ 10.66 m. As per the actual site, theoretical calculations and mine benefits preliminarily determined that the coal pillar width should be 11–12 m.

3.2. Optimization Analysis of Coal Pillar Width Based on Numerical Simulation

1. Numerical calculation model for different coal pillar widths

According to the actual geological production conditions of panel 3210 of the Wangpo mine and its adjacent areas, a FLAC^{3D} numerical calculation model was constructed, with the model size x × y × z = 300 m × 300 m × 100 m. The left and right boundaries were fixed in the model in the x-direction. The front and rear boundaries were fixed in the y-direction. The lower boundary was fixed in the z-direction. The upper boundary of the

model was a free edge. According to the coal seam's buried depth of 560 m, combined with the in situ stress test results in the mine's geological data, a load of 12.265 MPa was applied above the model to simulate the overburden acceleration of gravity of 9.81 m/s^2. The Mohr–Coulomb model was selected as the constitutive model. The mechanical parameters of the numerical model are presented in Table 2.

Table 2. Mechanical parameters of coal and rock strata.

| Rock Strata	K/GPa	G/GPa	C_m/MPa	φ_m/(°)	σ_{tm}/MPa	D/(kg·m^{-3})
Mudstone	10.0	6.0	1.4	24	1.3	2300
Limestone	13.5	8.1	2.55	31	2.5	2550
No. 3 coal seam	8.0	4.84	0.6	10	0.5	1440
Quartz sandstone	13.0	7.0	2.4	28	2.1	2500
No. 5 coal seam	8.0	4.84	0.6	10	0.5	1440
Sandy mudstone	10.0	6.0	1.6	25	1.4	2400
Fine-grained sandstone	15.0	9.2	2.6	30	2.4	2600

K is the bulk modulus, G is the shear modulus, C_m is the cohesion, σ_{tm} is the tensile strength, φ_m is the friction angle, and D is the density.

2. Analysis of distribution law of stress and plastic zone of surrounding roadway rock based on different coal pillar widths

According to the coal pillar of the original similar panel section in the Wangpo mine and the coal pillar retention engineering case of roadways along gob under similar conditions, the coal pillar width was set as 5, 8, 11, 14, and 17 m. The surrounding rock stress, plastic zone affected by the mining of adjacent panels, and the stability of the two entries were analyzed and compared. The coal pillar width was optimized based on the numerical simulation results. Figure 7 shows the vertical stress distribution and plastic zone distribution of the surrounding roadway rock with different coal pillar widths. At the same time, the stress on the two sides of the tailgate was monitored. The monitoring data mapping combines the stress distributions to more intuitively characterize the stress change law with different coal pillar widths.

Compared with the stress distribution in Figure 7, it can be seen that the excavation of the high-drainage roadway mainly changes the stress concentration range and value of the solid coal side of the tailgate and has little effect on the stress distribution of the coal pillar. When the coal pillar width was 5 m, the maximum concentrated stress value on the coal pillar was 39.47 MPa; when the coal pillar width increased to 8 m, the maximum concentrated stress value surged to 66.25 MPa. At this time, the concentrated stress area was still located in the center of the coal pillar, with a "single peak" distribution. When the coal pillar width was gradually increased to 11 m, an increase in the maximum concentrated stress value was not apparent. The high-stress area slowly presented a "double peak" distribution. The shallow surrounding rock at the coal pillar side of the tailgate gradually deviated away from the maximum concentrated stress area. Comparing the stress distribution of different coal pillar widths, it can be seen that on the premise of minimizing coal pillar loss, a slight increase in coal pillar width can reduce the stress value of the surrounding rock of the tailgate, but the effect is minimal.

It can be seen from the distribution of the plastic zone in Figure 7 that when the width of the coal pillar was 5 m and 8 m, the coal pillar was in a fully plastic state. When the width of the coal pillar increased to approximately 11 m, a stable elastic zone appeared in the center of the coal pillar. The coal body in this area is relatively complete, which is conducive to anchoring the anchor cable. The dense coal body prevents residual gas from flowing into panel 3210 from the adjacent gob. Based on the theoretical calculation and similar simulation results and combined with numerical simulation analysis, the coal pillar width was finally determined to be 11.5 m.
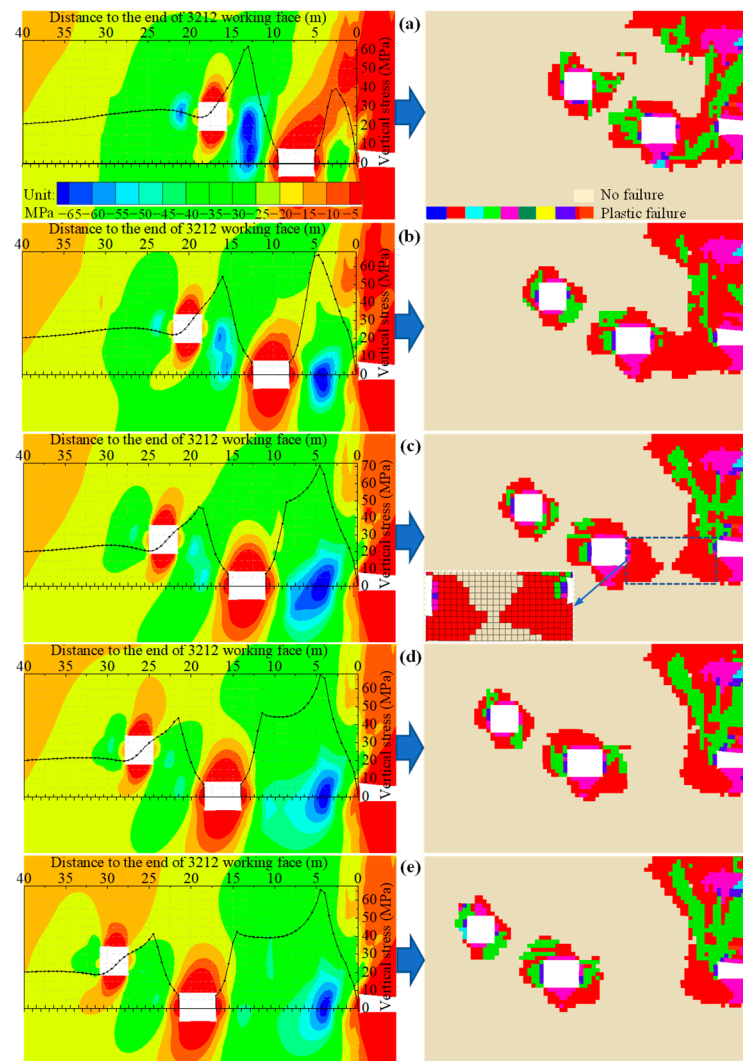
Figure 7. Vertical stress and plastic zone distribution of surrounding roadway rock with different coal pillar widths: (**a**) 5 m, (**b**) 8 m, (**c**) 11 m, (**d**) 14 m, (**e**) 17 m.

4. Analysis of Surrounding Rock Control Method of a Broken Coal Roadway Located in the Lower Position of a "Two-Entry in Different Layers" Arrangement and Adjacent to Gob in a Fully Mechanized Caving Face

### 4.1. Simulation Analysis of the Key Supporting Area of Tailgate-Surrounding Rock

It can be seen from the plasticity that the deviatoric stress considers the interaction of the maximum principal stress [40], intermediate principal stress, and minimum principal stress, which can scientifically reveal the relationship between the stress evolution of the surrounding roadway rock and the deformation of the surrounding rock. Among them, the maximum principal deviator stress plays a substantial role in the deformation of the surrounding rock in the stress tensor, with the following expression [41]:

$$D_1 = \sigma_1 - \frac{\sigma_1 + \sigma_2 + \sigma_3}{3} \tag{7}$$

where σ_i (i = 1, 2, 3) is the three principal stresses at one point, and $\sigma_1 > \sigma_2 > \sigma_3$.

Combined with the research contents of this paper, to effectively understand the distribution law of stress in the surrounding rock of the two-entry arrangement, the index of deviatoric stress is used to study the stress state of the surrounding rock, study and judge the complex support area of the surrounding rock, and then guide the surrounding rock support of the roadway. Figure 8 shows the contour of the deviatoric stress distribution of

the surrounding rock after the excavation of two entries (the width of the coal pillar is 11 m). Figure 8a shows that after excavating tailgate 3210, the coal pillar exhibits a high deviatoric stress area (zone A) in the shape of a parallelogram. The second high deviatoric stress area (zone B) was formed in the upper area of the left side of the tailgate. Zone B is distributed in an arc shape around the upper left corner of the roadway, approximately 1.5 m away from the roadway surface. Figure 8b shows that the third and fourth high deviatoric stress areas (Zone C and Zone D) are formed at the lower right corner and the upper left corner of the roadway after the excavation of the high-drainage roadway is completed. As shown in Figure 8c, the four high deviatoric stress areas (the peak values of deviatoric stress are 20.7, 16.5, 16.7, and 15.6 MPa) form a continuous high deviatoric stress zone along the diagonal direction of the two entries. The existence of high deviatoric stress in the surrounding rock can easily cause fragmentation and instability of the surrounding rock, leading to accidents.
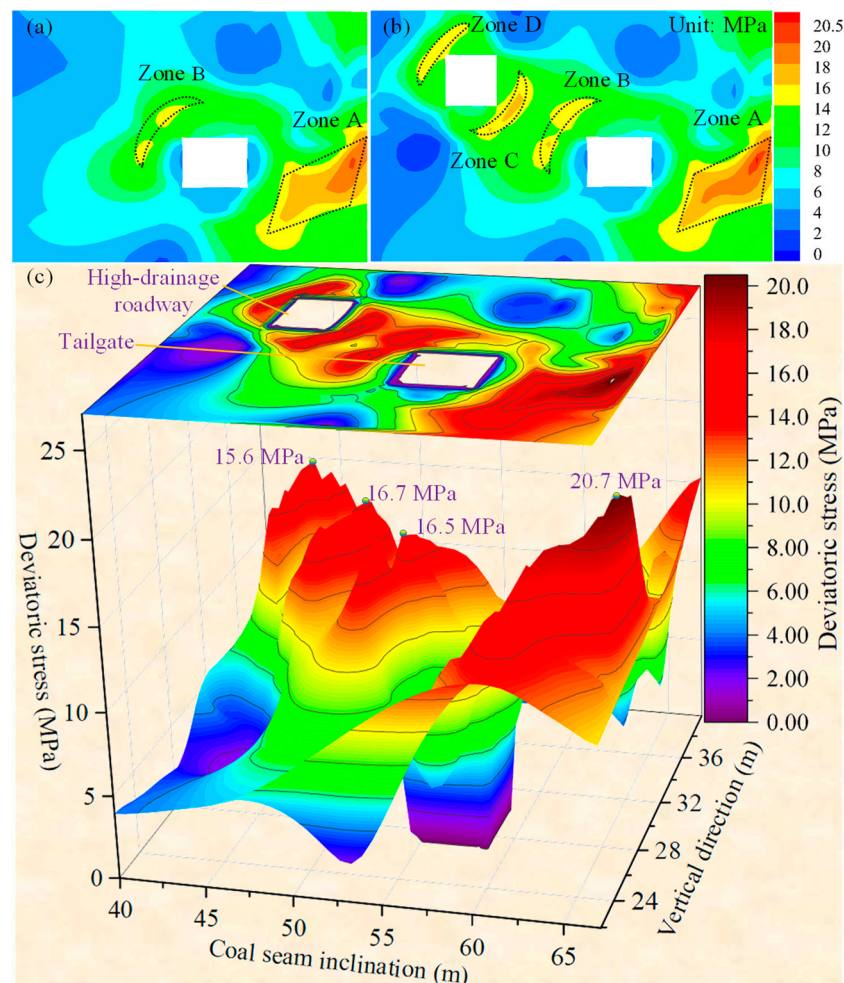
Figure 8. Deviatoric stress distribution in surrounding rock of a two-entry arrangement: (**a**) Before excavation of the high-drainage roadway, (**b**) after excavation of the high-drainage roadway, (**c**) peak values of deviatoric stress in rock surrounding the two entries.

According to the distribution of the plastic zone of the rock surrounding the two-entry arrangement in Figure 7c, the depth of the plastic zone on the pillar side of the tailgate is 4.5 m and the depth of the plastic zone of the solid coal side of the tailgate is 3.0 m. The depth of the plastic zone of the roof is 2.5 m. The surrounding rock at the upper left corner of the tailgate is in a plastic state. In summary, the main failure areas of the rock surrounding the tailgate are mainly concentrated in three points: the coal pillar side, the solid coal side, and the upper left corner of the tailgate.

Based on the analysis of the distribution of the high deviatoric stress area and the plastic zone of the surrounding rock, the surrounding rock of tailgate 3210 will form two key supporting areas: the section coal pillar of the gob-side entry and the coal–rock pillar between the two entries, especially in the diagonal coal–rock pillar area of the two entries.

4.2. Main Control of the Surrounding Rock in the Tailgate

Combined with the geological production conditions of panel 3210 and the abovementioned analysis results, considering the critical areas of surrounding roadway rock control and surrounding rock strength, the surrounding rock supporting area of the two entries in different layers in a fully mechanized caving face is spatially divided into "two pillars, three zones, and three parts", as shown in Figure 9.
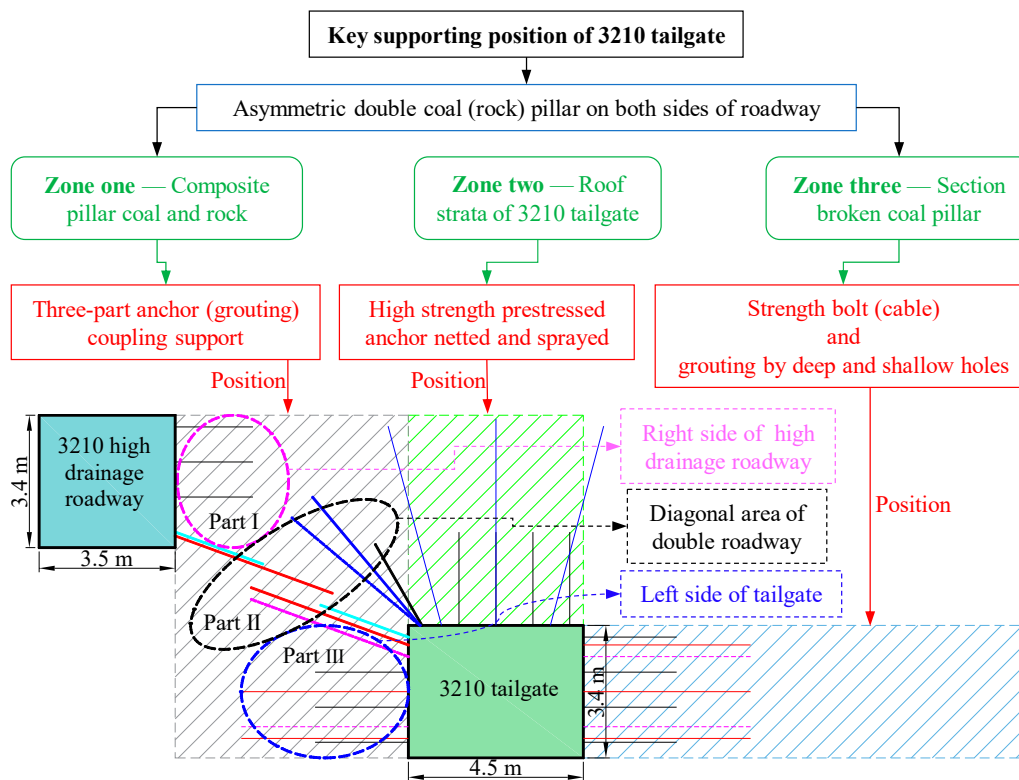

Figure 9. Idea of surrounding rock zoning support in tailgate.

"Two pillars" refers to the coal–rock pillar between the two entries and the broken coal pillars adjacent to the gob and "three zones" refers to the solid coal side, roof, and coal pillar side of the tailgate. "Three parts" refers to the characteristics of coal and rock mass structure, failure characteristics, and deviatoric stress distribution. The coal–rock pillar between the two entries is divided into three parts for graded support: part I on the right side of the high-drainage roadway, part II on the diagonal area of the two entries, and part III on the left side of the tailgate.

Different support methods are adopted for other areas according to the control design approach of "two pillars, three zones, and three parts". The primary control ideas are as follows: 1. Anchor bolt (cable) supports with different support parameters are adopted for the "three zones" of surrounding roadway rock, and the anchorage zone of anchor bolt–surrounding rock coupling is formed through anchor bolt (cable) support to improve the surrounding rock environment [42,43]; 2. To improve the bearing capacity of the broken coal and rock mass, the solid coal side (Part III) of the tailgate and the broken coal pillar-adjacent gob are supported by grouting. In addition, the diagonal coal–rock pillar area of the two entries (Part II) is broken owing to the interbedding of mudstone and sandy mudstone, high deviatoric stress, and the disturbance of two-entry excavation. Grouting

support is also required for part II; 3. The diagonal coal–rock pillar area of the two entries (Part II) is the most unstable area caused by the two-entry arrangement, which is the critical point of support. Anchor bolts (cables) with different included angles were arranged in this area to form an overlapping area of anchor bolt (cable) support. Combined with the grouting support, the anchor bolts (cables), slurry, and coal-and-rock mass form an interactive linkage structure, significantly improving the support strength in this area.

5. Engineering Practice

5.1. Surrounding Rock Control Scheme and Support Parameters

According to the above analysis, combined with the actual situation of the mine, the technical scheme of combined anchor–net–grout support in the surrounding rock of the tailgate was determined. A schematic drawing of the support is shown in Figure 10, and the support parameters are as follows:

1. Roof of the tailgate: the roof adopted a $\varphi 22 \times 2400$ mm left-hand rolling-thread steel bolt without longitudinal reinforcement (denoted by X bolt), and the spacing and row spacing were 950×1000 mm. In addition, SKP22-1/1860-5300 high-strength and low-relaxation steel strand anchor cables (denoted by Y anchor cables) were also used, and the spacing and row spacing were 1400×1000 mm;

2. Solid coal side of the tailgate: the roadway side adopted an X bolt, the included angle between the first bolt on the upper side and the horizontal line was $20°$, the spacing and row spacing were 900×1000 mm, and one $\varphi 28 \times 2400$ mm hollow spiral grouting bolt (denoted by X_1 bolt) was used when two X bolts were spaced along the axial direction of the roadway. In addition, a Y anchor cable was used, arranged in 3-2-3 along the axial direction of the roadway. When there were two anchor cables in each row, the spacing was 1800 mm, and when there were three anchor cables in each row, the spacing was 1200 mm, arranged perpendicular to the roadway side. The row spacing of the anchor cables was 1000 mm. One $\varphi 29 \times 5300$ mm grouting anchor cable (denoted by Y_1 anchor cable) was used when two Y anchor cables were spaced along the axial direction of the roadway;

3. Coal pillar side of the tailgate: the roadway side adopted an X bolt, the spacing and row spacing were 900×1000 mm, and an X_1 bolt was used when two X bolts were spaced along the axial direction of the roadway. In addition, a Y anchor cable was used, arranged in 3-2-3 along the axial direction of the roadway. When there were two anchor cables in each row, the spacing was 1800 mm, and when there were three anchor cables in each row, the spacing was 1200 mm, arranged perpendicular to the roadway side. The row spacing of the anchor cables was 1000 mm. A Y_1 anchor cable was used when two Y anchor cables were spaced along the axial direction of the roadway;

4. Diagonal coal–rock pillar area of the two entries: the diagonal coal–rock pillar area of the two entries (Part II) was divided into three parts. 1. Roof of the tailgate: the included angle between the leftmost bolt of the roof and the vertical line was $30°$, and an X_1 bolt was used when two X bolts were spaced along the axial direction of the roadway. In addition, an anchor cable with a length of 4300 mm was added to the roadway roof (300 mm away from the solid coal side), and a Y_1 anchor cable was used when two Y anchor cables were spaced along the axial direction of the roadway. When there were three anchor cables in each row, the roof anchor cable was located in the same row, and the included angle with the vertical line was $50°$. When there were two anchor cables, the roof anchor cable was found in the same row, and the included angle with the vertical line was $40°$; 2. Solid coal side of the tailgate: the included angle between the uppermost bolt (an anchor cable) of the solid coal side and the horizontal line was $20°$, and an X_1 bolt (a Y_1 anchor cable) was used when two X bolts (Y anchor cables) were spaced along the axial direction of the roadway; 3. Right side of high-drainage roadway: the included angle between the lowest point of the right side of the high-drainage roadway and the horizontal line was $20°$, and

one X_1 bolt was used when two X bolts were spaced along the axial direction of the roadway. A Y anchor cable was added to the right side of the high-drainage roadway (300 mm away from the floor of the high-drainage roadway), and the included angle with the horizontal line was 20°.
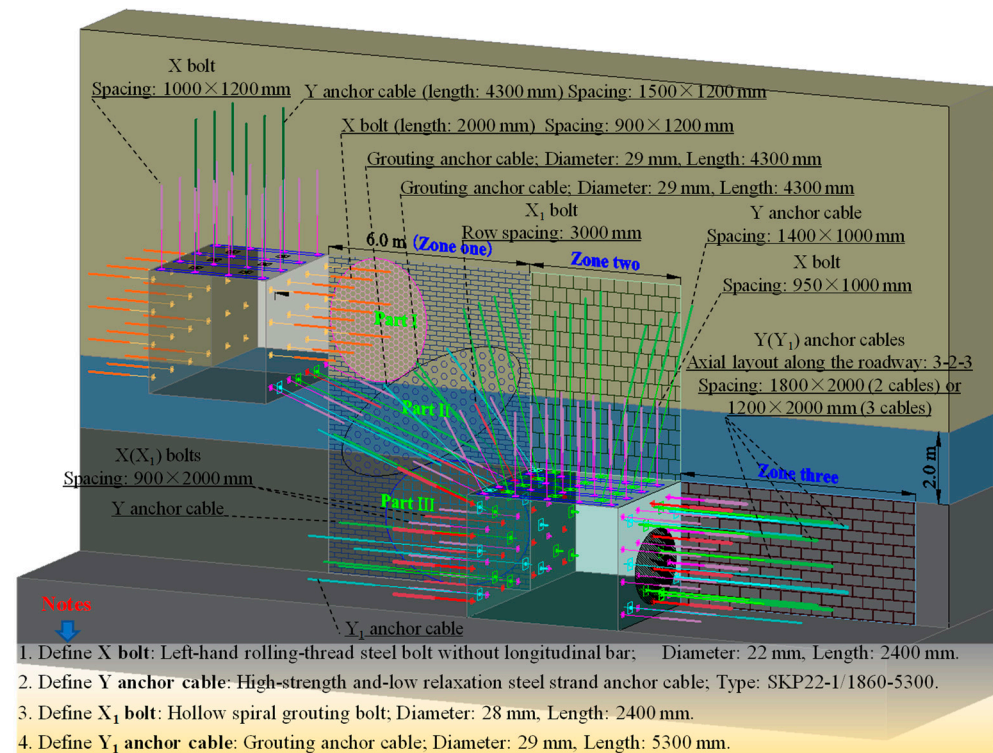

Figure 10. Schematic drawing of surrounding rock support parameters of the tailgate.

5.2. Mine Pressure Monitoring and Coal Grouting Strength Test

To evaluate the reliability of the tailgate 3210 support scheme and understand the working state of the roadway support structure, the surrounding rock surface displacement and anchor bolts (cables) anchoring force of the test section (the support scheme studied in this paper, the length of the test section is 100 m, and the test section is arranged 1000 m to 1100 m away from the open-off cut of the 3210 panel) and ordinary support section (the original design support scheme of the mine) of the tailgate 3210 were monitored. In addition, the surrounding rock grouting effectively solidified the tailgate's broken coal body, improved the coal body's strength and integrity, and provided an excellent anchor body for anchor bolt (cable) support. To understand the time–strength effect of the grouting coal body, field sampling was carried out at the coal pillar side of the tailgate 3210, and the coal grouting body strength experiment was carried out in the laboratory.

5.2.1. Strength Test of Broken Coal by Grouting

To study the strength law of the broken coal body of the coal pillar side at different grouting times, a side-limit loading test for a standard laboratory specimen, as shown in Figure 11a,b, was designed to simulate the stress environment of the coal pillar side grouted coal body through a uniaxial compression testing machine and confined plate.
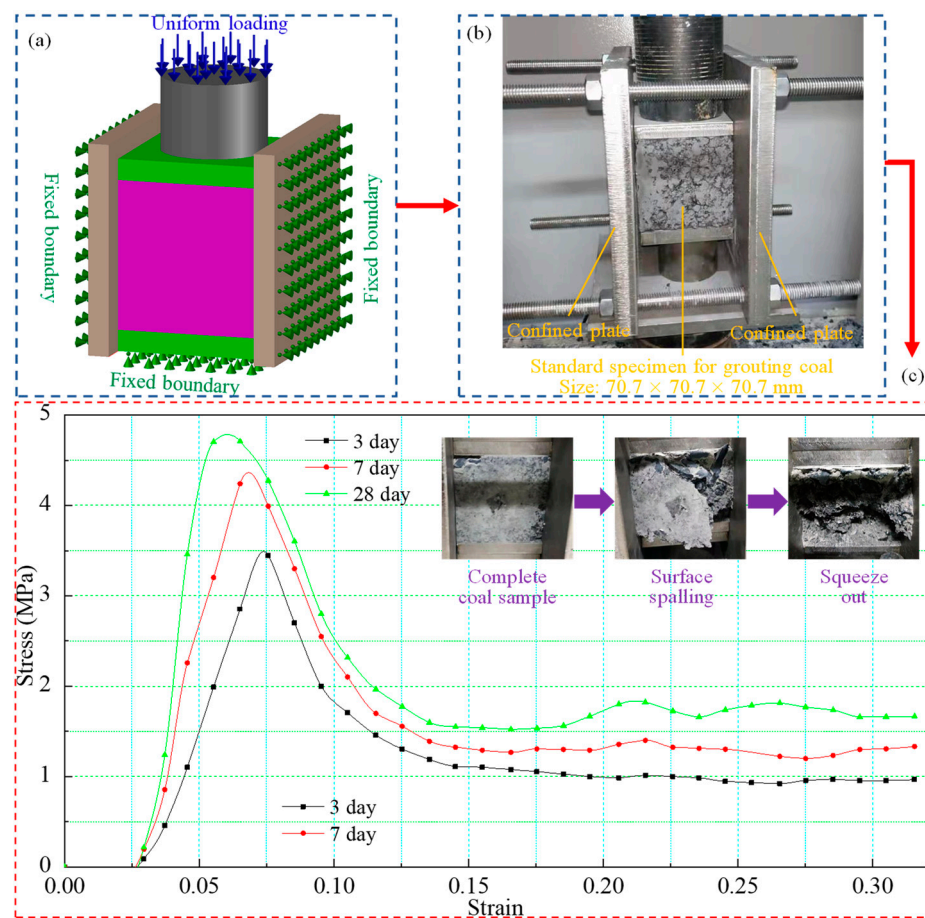
Figure 11. Side-limit experiment and results: (**a**) Side-limited loading principle, (**b**) laboratory measurement, (**c**) stress–strain curves of coal specimens at different grouting times.

Uniaxial compression tests were performed on standard specimens (70.7 mm × 70.7 mm × 70.7 mm) with different grouting times. Figure 11a shows the specimens' loading conditions. The upper and lower boundaries of the specimens were used to apply uniform loading. The loading rate is 1 kN/s, the left and right boundaries were fixed, and the front and rear boundaries were free boundaries. The results are shown in Figure 11c. After 28 days of grouting, the final strength of the grouted coal specimen was 4.7 MPa. When the grouting time was 3 days, the grouted coal strength reached 72.3% of the peak strength, whereas when the grouting time was 7 days, the grouted coal strength achieved 90.2% of the peak strength. This shows that grouting can quickly improve the strength of coal and transform coal around the roadway into a relatively complete supporting and bearing structure in a short time. Complete coal grouting can provide a better support environment for the anchor bolts (cables), which are conducive to maximizing its support effect.

5.2.2. Surface Displacement Monitoring of Surrounding Roadway Rock

The cross-point method was used to monitor roadway displacement. After excavating tailgate 3210, the surrounding rock surface displacement monitoring results were drawn into a time–displacement curve, as shown in Figure 12a. The relation curve between the displacement of the surrounding rock in the front section of the 3210 panel and the distance from the panel is shown in Figure 12b. According to Figure 12a, the roadway deformation tends to be stable approximately 44 days after the support is completed. The maximum displacements of the roof-to-floor distance of the ordinary support and test sections were 178 mm and 88 mm, respectively. The maximum displacements of the two sides were 133 mm and 64 mm, respectively, and the displacements of the roof-to-floor distance and two sides were reduced by 50.6% and 51.9%, respectively. As shown in Figure 12b,

in the mining stage of panel 3210, the displacement of the surrounding roadway rock increased significantly owing to the influence of advancing abutment pressure caused by fully mechanized caving mining. Most of the surrounding roadway rock deformation was formed within 48 m of the panel, and the roof-to-floor displacement was still more significant than that of the two sides. The maximum displacements of the roof-to-floor distance of the ordinary support and test sections were 733 mm and 203 mm, respectively. The maximum displacements of the two sides were 689 mm and 174 mm, respectively, and the displacements of the roof-to-floor distance and two sides are reduced by 72.3% and 74.7%, respectively. From the displacement point of view, the new support scheme effectively limits the displacement of the surrounding roadway rock.
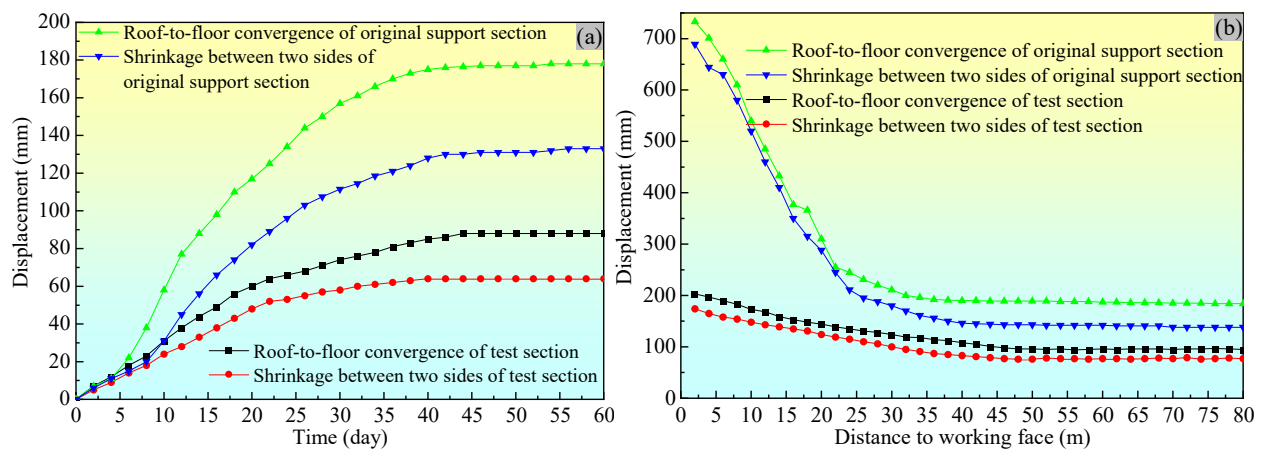
Figure 12. Displacement curves of the rock surrounding tailgate 3210 in test section and ordinary support section. (**a**) Displacement–time curves of tailgate 3210 after excavation. (**b**) Displacement curves in the front section of the tailgate.

Overall, the deformation of the surrounding roadway rock was within the controllable range, and the anchoring force of the anchor bolts (cables) met the anchoring requirements. The anchor bolts (cables) did not break in the mining stage owing to excessive tensile anchor force. The qualification rate was very high, the construction quality of the roadway support was good, the support system was reliable, and the control effect of the surrounding roadway rock was sound.

6. Conclusions

1. Tailgate 3210 and the high-drainage roadway in the Wangpo mine form a unique two-entry arrangement in different layers, and the fragmentation characteristics of the No. 3 coal seam, which makes weak, asymmetrically strong double coal–rock pillars form on both sides of tailgate 3210, has a significant impact on the stability of tailgate 3210;

2. Based on the "internal and external stress field" theory, the position of the main roof fracture line was calculated, combined with a similarity simulation test and numerical simulation analysis. It was concluded that the reasonable width for the coal pillar on the side of tailgate 3210 is 11.5 m;

3. Through the analysis of the distribution of the high deviatoric stress areas and plastic zones of the surrounding rock, the key supporting area of surrounding rock of tailgate 3210 was defined, the surrounding rock control design approach of "two pillars, three zones, and three parts" was determined, and the support parameters of the rock surrounding the two entries were determined. Through field tests, the control effect of the surrounding rock of the roadway was adequate, and the support scheme can meet the needs of regular production.

References

1. Azadeh, A.; Tarverdian, S. Integration of genetic algorithm, computer simulation and design of experiments for forecasting electrical energy consumption. *Energy Policy* **2007**, *35*, 5229–5241. [CrossRef]
2. Aydin, G. Production modeling in the oil and natural gas industry: An application of trend analysis. *Petrol. Sci. Technol.* **2014**, *32*, 555–564. [CrossRef]
3. Aydin, G. Forecasting natural gas production using various regression models. *Petrol. Sci. Technol.* **2015**, *33*, 1486–1492. [CrossRef]
4. Aydin, G.; Karakurt, I.; Aydiner, K. Analysis and mitigation opportunities of methane emissions from energy sector. *Energy Source Part A* **2012**, *34*, 967–982. [CrossRef]
5. Wu, Q.; Tu, K. Analysis on the dual constraints of energy and environment to the development of China and countermeasures. *Sci. Bull.* **2019**, *15*, 1535–1544. [CrossRef]
6. Zhang, B.S.; Wang, P.F.; Cui, S.Q.; Fan, M.Z.; Qiu, Y.M. Mechanism and surrounding rock control of roadway driving along gob in shallow-buried, large mining height and small coal pillars by roof cutting. *J. China Coal Soc.* **2021**, *46*, 2254–2267.
7. Huang, S.J.; Zhao, G.M.; Meng, X.R.; Cheng, X.; Gu, Q.H.; Liu, G.; Zhu, S.K. Development of cement-based grouting material for reinforcing narrow coal pillars and engineering applications. *Processes* **2022**, *10*, 2292. [CrossRef]
8. Xu, X.H.; He, F.L.; Li, X.B.; He, W.R. Research on mechanism and control of asymmetric deformation of gob side coal roadway with fully mechanized caving mining. *Eng. Fail. Anal.* **2021**, *120*, 105097. [CrossRef]
9. Xie, S.R.; Wang, E.; Chen, D.D.; Sun, Y.H.; Cheng, Q.; Ji, C.W.; Yan, Z.Q.; Xiao, H.B. Failure analysis and control mechanism of gob-side entry retention with a 1.7-m flexible-formwork concrete wall: A case study. *Eng. Fail. Anal.* **2020**, *117*, 104816. [CrossRef]
10. Hou, C.J.; Li, X.H. Stability principle of big and small structures of rock surrounding roadway driven along goaf in fully mechanized top coal caving face. *J. China Coal Soc.* **2001**, *26*, 1–7.
11. Bai, J.B. *Surrounding Rock Control of Entry Driven along Goaf*; China University of Mining and Technology Press: Xuzhou, China, 2006.
12. He, W.R.; He, F.L.; Chen, D.D.; Chen, Q.K. Pillar width and surrounding rock control of gob-side roadway with mechanical caved mining in extra-thick coal seams under hard-thick main roof. *J. Min. Saf. Eng.* **2020**, *37*, 349–358.
13. Hua, X.Z.; Liu, S.; Liu, Z.H.; Zha, W.H.; Li, Y.F. Research on strata pressure characteristic of gob-side entry driving in island mining face and its engineering application. *Chin. J. Rock Mech. Eng.* **2011**, *30*, 1646–1651.
14. Yang, J.P.; Cao, S.G.; Li, X.H. Failure laws of narrow pillar and asymmetric control technique of gob-side entry driving in island coal face. *Int. J. Min. Sci. Technol.* **2013**, *23*, 267–272. [CrossRef]
15. Wang, D.C.; Wang, Q.; Li, S.C.; Wang, F.Q.; Ruan, G.Q.; Shao, H.; Liu, W.J.; Wang, X. Mechanism of rock deformation and failure and its control technology of roadway driving along next goaf in fully mechanized top coal caving face of deep mines. *J. Min. Saf. Eng.* **2014**, *31*, 665–673.
16. Yin, Q.; Jing, H.W.; Dai, D.P.; Zhu, T.T.; Zhao, H.H.; Meng, B. Cable-truss supporting system for gob-side entry driving in deep mine and its application. *Int. J. Min. Sci. Technol.* **2016**, *26*, 885–893. [CrossRef]
17. Yu, W.J.; Li, K.; Liu, Z.; An, B.F.; Wang, P.; Wu, H. Mechanical characteristics and deformation control of surrounding rock in weakly cemented siltstone. *Environ. Earth Sci.* **2021**, *80*, 337. [CrossRef]
18. Zhang, H.W.; Wan, Z.J.; Zhang, Y.; Ma, C.Y.; Zhang, J.; Liu, S.F.; Ge, L.J. Deformation mechanism of narrow coal pillar in the fully-mechanized gob-side entry with incompletely stable overlying strata. *J. Min. Saf. Eng.* **2016**, *33*, 692–698.
19. Zhang, Y.; Wan, Z.J.; Li, F.C.; Zhou, C.B.; Zhang, B.; Guo, F.; Zhu, C.T. Stability of coal pillar in gob-side entry driving under unstable overlying strata and its coupling support control technique. *Int. J. Min. Sci. Technol.* **2013**, *23*, 193–199. [CrossRef]
20. Zhang, D.S.; Wang, H.S.; Ma, L.Q. Two-step gob-side entry driving technology of pre-build artificial side substitute for narrow coal pillar. *J. China Coal Soc.* **2010**, *35*, 1589–1593.
21. Yuan, H.H.; Shan, R.L.; Su, X.G. Deformation characteristics and stability control of a gateroad in fully mechanized mining with large mining height. *Arab. J. Geosci.* **2018**, *11*, 767. [CrossRef]
22. Gao, X.; Zhang, S.; Zi, Y.; Pathan, S.K. Study on optimum layout of roadway in close coal seam. *Arab. J. Geosci.* **2020**, *13*, 746. [CrossRef]

23. Guo, J.G.; Wang, W.G.; Yue, S.S.; He, F.L.; Gao, M.M.; Xie, S.R. Surrounding rock control mechanism and its application of gob-side driving entry in extra thick coal seam. *J. China Coal Soc.* **2017**, *42*, 825–832.

24. Zhang, N.; Li, X.H.; Gao, M.S. Pretensioned support of roadway driven along next gob and heading adajacent advancing coal face and its application. *Chin. J. Rock Mech. Eng.* **2004**, *23*, 2100–2105.

25. Jawed, M.; Sinha, R.K. Design of rhombus coal pillars and support for roadway stability and mechanizing loading of face coal using SDLs in a steeply inclined thin coal seam-a technical feasibility study. *Arab. J. Geosci.* **2018**, *11*, 415. [CrossRef]

26. Wang, M.; Bai, J.B.; Wang, X.Y.; Chen, B.; Han, Z.T. Stability and control technology of overlying structure in gob-side entry driving roadways of deep inclined coal seam. *J. Min. Saf. Eng.* **2015**, *32*, 426–432.

27. Xie, S.R.; Pan, H.; Zeng, J.C.; Wang, E.; Chen, D.D.; Zhang, T.; Peng, X.J.; Yang, J.H.; Chen, F.; Qiao, S.X. A case study on control technology of surrounding rock of a large section chamber under a 1200-m deep goaf in Xingdong coal mine, China. *Eng. Fail. Anal.* **2019**, *104*, 112–125. [CrossRef]

28. Bai, J.B.; Shen, W.L.; Guo, G.L.; Wang, X.Y.; Yu, Y. Roof deformation, failure characteristics, and preventive techniques of gob-side entry driving heading adjacent to the advancing working face. *Rock Mech. Rock Eng.* **2015**, *48*, 2447–2458. [CrossRef]

29. Li, L.; Bai, J.B.; Wang, X.Y. Rational position and control technique of roadway driving along next goaf in fully mechanized top coal caving face. *J. China Coal Soc.* **2012**, *37*, 1564–1569.

30. Yu, Y.; Bai, J.-B.; Wang, X.Y.; Zhang, L.Y. Control of the surrounding rock of a goaf-side entry driving heading mining face. *Sustainability* **2020**, *12*, 2623. [CrossRef]

31. Xie, G.X.; Yang, K.; Chang, J.C. Effect of coal pillar width on the stress distribution law of surrounding rocks in fully mechanized top-coal caving mining face. *J. Univ. Sci. Technol. Beijing* **2006**, *28*, 1005–1008.

32. Wang, Q.W.; Feng, H.; Tang, P.; Peng, Y.T.; Li, C.A.; Jiang, L.S.; Mitri, H.S. Influence of yield pillar width on coal mine roadway stability in western China: A case study. *Processes* **2022**, *10*, 251. [CrossRef]

33. Xie, S.R.; Wang, E.; Chen, D.D.; Jiang, Z.S.; Li, H.; Liu, R.P. Collaborative control technology of external anchor-internal unloading of surrounding rock in deep large-section coal roadway under strong mining influence. *J. China Coal Soc.* **2022**, *47*, 1946–1957.

34. Wu, Y.Z. Study on de-stressing mechanism of directional hydraulic fracturing to control deformation of reused roadway in longwall mining with two gate road layout and its practices. *China Coal Res. Inst.* **2018**, 12.

35. Sun, G.Z. Advance in rockmass mechanics—Rockmass structural mechanics. *Chin. J. Rock Mech. Eng.* **1991**, *10*, 112–116.

36. Xie, S.R.; Pan, H.; Chen, D.D.; Zeng, J.C.; Song, H.Z.; Cheng, Q.; Xiao, H.-B.; Yan, Z.Q.; Li, Y.H. Stability analysis of integral load-bearing structure of surrounding rock of gob-side entry retention with flexible concrete formwork. *Tunn. Undergr. Space Technol.* **2020**, *103*, 103492. [CrossRef]

37. Song, Z.Q. *Practical Method of Mine Pressure Control*; China University of Mining and Technology Press: Xuzhou, China, 1988; pp. 122–130.

38. Qian, M.G.; Shi, P.W. *Mine Pressure and Strata Control*; China University of Mining and Technology Press: Xuzhou, China, 2003; pp. 76–79.

39. Shu, Z.H. Simulation experimental study on surface subsidence and overburden movement law under thick loose mining conditions. Ph.D. Thesis, Anhui University of Science and Technology, Huainan, China, 2019.

40. Xia, Z.G. *Plasticity*; Tongji University Press: Shanghai, China, 1991; pp. 18–20.

41. Xie, S.R.; Pan, H. Surrounding rock deviatoric stress difference evolution and control of gob-side entry driving in deep mining. *China Min. Mag.* **2018**, *27*, 98–102.

42. Yu, W.J.; Wu, G.S.; Pan, B.; Wang, C.L.; Li, K.; Liao, Z. Laboratory and field investigations of different bolting configurations for coal mine roadways in weak coal strata. *Bull. Eng. Geol. Environ.* **2021**, *80*, 8995–9013. [CrossRef]

43. Yu, W.J.; Wu, G.S.; Pan, B.; Wu, Q.H.; Liao, Z. Experimental investigation of the mechanical properties of sandstone-coal-bolt specimens with different angles under conventional triaxial compression. *Int. J. Geomech.* **2021**, *21*, 04021067. [CrossRef]